

RSC Advances



This is an *Accepted Manuscript*, which has been through the Royal Society of Chemistry peer review process and has been accepted for publication.

Accepted Manuscripts are published online shortly after acceptance, before technical editing, formatting and proof reading. Using this free service, authors can make their results available to the community, in citable form, before we publish the edited article. This *Accepted Manuscript* will be replaced by the edited, formatted and paginated article as soon as this is available.

You can find more information about *Accepted Manuscripts* in the [Information for Authors](#).

Please note that technical editing may introduce minor changes to the text and/or graphics, which may alter content. The journal's standard [Terms & Conditions](#) and the [Ethical guidelines](#) still apply. In no event shall the Royal Society of Chemistry be held responsible for any errors or omissions in this *Accepted Manuscript* or any consequences arising from the use of any information it contains.



Journal Name

ARTICLE

Growth of Fe₃O₄ Nanosheet arrays on Graphene by a Mussel-Inspired Polydopamine Adhesive for Remarkable Enhancement in Electromagnetic Absorptions

Received 00th January 20xx,
Accepted 00th January 20xx

DOI: 10.1039/x0xx00000x

www.rsc.org/

Fanbin Meng*, Wei Wei, Jingjing Chen, Xiangnan Chen, Xiaoling Xu, Man Jiang, Yong Wang, Jun Lu and Zuowan Zhou*

Fe₃O₄ nanosheet arrays grown on both surfaces of graphene can be achieved by combining a mussel-inspired polydopamine adhesive and ethylene glycol-mediated process. Polydopamine is utilized not only as an efficient linker molecule that binds Fe₃O₄ nanosheets to the graphene, but also as a carbon source during heat treatment to yield the three dimensional (3D) graphene@carbon@Fe₃O₄ nanosheet arrays architecture. After the growth of Fe₃O₄ nanosheet arrays with accompanied reduction of graphene oxide into graphene, the 3D architecture exhibits outstanding microwave absorption properties. The simulated value of maximum reflection loss can reach -52.8 dB at 9.5 GHz with a sample thickness of 2.7 mm. The improved absorption capacity arises from the synergy of dielectric loss and magnetic loss, as well as the enhancement of multiple interfaces among graphene, carbon and Fe₃O₄ nanosheets. Furthermore, the synthesis strategy presented here can be expanded as a facile approach to synthesizing related graphene-based 3D nanostructures for functional design and applications.

1. Introduction

Recently, great efforts have been made towards development of high efficiency and lightweight microwave absorbers to effectively eliminate the increasing adverse electromagnetic interference and radiation problems.¹⁻⁴ In particular, graphene-based nanostructures are becoming more and more attractive utilized in electromagnetic (EM) absorptions, including graphene-supported or -wrapped nanostructures.⁵⁻¹⁰ Firstly, graphene promises to be a superior building block for constructing electromagnetic wave absorbers, owing to its remarkable physical properties including large surface

area, high conductivity and good thermal conductivity.¹¹ Taking advantage of the benefits of conductive graphene and the introduced other lossy materials, as well as the interfacial and synergistic effects, the graphene-based nanostructures may result in strong EM absorption properties. Ren et al developed a new strategy, i.e., a seed-assistant method, to fabricate three dimensional (3D) SiO₂@Fe₃O₄ core/shell nanorod array/graphene architecture, and the maximum reflection loss reached -31.9 dB with a sample thickness of 2.5 mm.¹² Li et al. reported a single polyol method to fabricate graphene/Fe₃O₄ hybrids with a maximum reflection loss of -30.1 dB at 1.48 mm matching thickness.¹³ Chen et al. introduced a new method for the preparation of graphene/polyaniline hybrids using a one-step intercalation polymerization of aniline inside the expanded graphite, and the results showed that the poor EM absorption properties of graphene could be significantly improved after the separation of graphite into graphene based hybrids. The maximum reflection loss reached -36.9 dB at 10.3 GHz with the thickness of 3.5 mm.¹⁴ However, the intrinsic poor impedance matching in such graphene/polymer systems hinders further improvement of application performances. Similarly, graphene decorated with inorganic nanocrystals generally aggregate with uneven distribution, leading to possible "dead areas" with null components, which also reduces the EM absorption properties. Therefore, design of a facile synthesis that ensures lossy nanocrystals uniformly decorated on the whole of the graphene nanosheets without aggregation is urgently needed.

Herein, we developed an efficient multi-step conversion approach to growing Fe₃O₄ nanosheets on the surfaces of graphene to form 3D graphene@Fe₃O₄ nanosheet architectures. In order to ensure the Fe₃O₄ nanosheets grow uniformly on the both surfaces of graphene, polydopamine (PDA) was utilized to act as an efficient linker molecule that binds Fe₃O₄ nanosheets to the graphene, inspired by the adhesion mechanism of mussels.¹⁵ Furthermore, the PDA can also act as a carbon source during heat treatment to yield 3D graphene@carbon@Fe₃O₄ nanosheet arrays architectures. Due to the special morphology, multi-interfacial polarization and impedance matching, the 3D graphene@carbon@Fe₃O₄ nanosheet

^a Key Laboratory of Advanced Technologies of Materials (Ministry of Education), School of Materials Science and Engineering, Southwest Jiaotong University, Chengdu 610031, China

*Corresponding Authors: mengfanbin_wing@126.com, zwzhou@home.swjtu.edu.cn

Electronic Supplementary Information (ESI) available: [SEM images of GO@iron alkoxide, the details about the formation of RGO@PDA@iron alkoxide nanosheet arrays, XRD pattern and Raman spectra of samples, frequency dependence of complex permeability and complex permittivity for GO and RGO@PDA, respectively, frequency dependence of $\mu''(\mu')^{-2}f^{-1}$ for graphene@carbon@Fe₃O₄.

arrays exhibited very good EM absorption properties, including strong attenuation to EM wave and lightweight characteristics.

2. Experimental section

2.1 Preparation of graphene@carbon@Fe₃O₄ nanosheet arrays

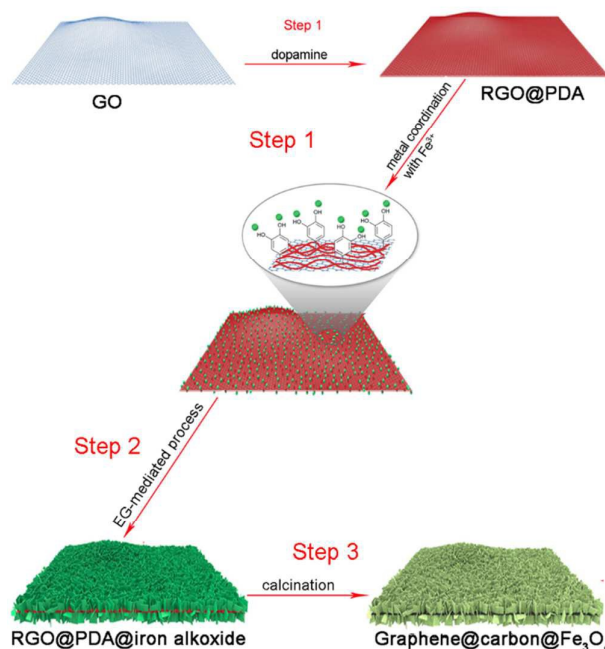
RGO@PDA was prepared by the simultaneous reduction of GO with dopamine hydrochloride and the self-polymerization of dopamine according to the reference.¹⁵ Then, RGO@PDA (10 mg) was dispersed into ethylene glycol (100 mL) with ultrasonication, and then FeCl₃·6 H₂O (0.6 g), urea (1.5 g) were added. This mixture was stirred at 50 °C for 2 h. Next, the solution was subsequently heated and refluxed at ~195 °C. When the mixture turned green, indicating the formation of iron alkoxide on the RGO@PDA. After further 5 min, the reaction was stopped and the mixture was cooled to room temperature. The precipitates were separated by centrifugation, washed with pure ethanol and dried in vacuum at 40 °C for 12 h. Last, the precipitates were calcined at 500 °C for 3 h under an argon atmosphere to obtain the final composites of graphene@carbon@Fe₃O₄.

2.2 Characterization

The morphologies were characterized on a field emission scanning electron microscopy (FE-SEM, JEOL, JSM-7001F) and a transmission electron microscopy (TEM, JEOL, JEM-2100F). X-ray diffraction (XRD) analyses were carried out on a Philips X'Pert PRO X-ray diffractometer with a CuK α radiation. The Raman spectra for the samples were obtained on a Laser Raman spectroscopy (InVia, RENISHAW) using a 514 nm argon ion laser. The complex permeability and permittivity were measured on a vector network analyzer (AV3618, CETC, China) in the frequency of 2-18 GHz. The samples were mixed with wax and prepared as the toroidal shape with an outer diameter of 7.0 mm, an inner diameter of 3.04 mm and a thickness of 3.0 mm. The mass ratios of the samples to wax were set to be 3:7.

3. Results and discussion

The processes involved in the formation of the 3D architecture, are illustrated in Scheme 1. First, graphene oxide (GO) was modified by PDA, leading to the reduction of GO into reduced graphene oxide (RGO). Importantly, the coated PDA can absorb and immobilize the Fe³⁺ by the strong coordination ability of the catechol groups,^{16,17} resulting in forming metal nanoparticles by an *in situ* nucleation (step 1). Next, these nanoparticles served as "seeds" for the growth of iron alkoxide nanosheets on the surfaces of RGO@PDA under the ethylene glycol (EG)-mediated process (step 2). Finally the 3D graphene@carbon@Fe₃O₄ nanosheet arrays can be obtained by a calcination of the RGO@PDA@iron alkoxide (step 3).



Scheme 1. The growth processes of the 3D graphene@carbon@Fe₃O₄ nanosheet arrays.

Fig. 1a and b shows the morphologies of RGO@PDA@iron alkoxide after the EG-mediated process by scanning electron microscopy (SEM). Growing nanosheets on both surfaces of RGO@PDA can be clearly found, forming interesting 3D architectures (Fig. 1a), and the iron alkoxide nanosheets are mostly grown upright with close and homogeneous on the RGO@PDA support as shown in Fig. 1b. The further investigations also revealed that the PDA used in the current system played an important role in the formation of such sheet-like structures, since only the aggregation of Fe₃O₄ nanosheets with flower-like morphology would be formed without the PDA coating on the GO surface (Figure S1, ESI[†]). Additionally, each reaction stage was also traced to investigate the growth mechanism of such architecture by SEM (Figure S2, ESI[†]). After thermal treatment, the 3D graphene@carbon@Fe₃O₄ nanosheet arrays were obtained and still maintain their original morphology (Fig. 1c). However, the size of the nanosheets decreases obviously, and many pores present in the nanosheets, due to the phase transformation of iron alkoxide to Fe₃O₄ (Fig. 1d). Such an interesting structure was also viewed under transmission electron microscopy (TEM; Fig. 1e), and the diffraction rings in the SAED pattern (inset of Fig. 1e) correspond to (220), (311), (400), (511) and (440) crystalline planes of Fe₃O₄. Furthermore, clear lattice fringes are observed in the high resolution TEM (HRTEM) image (Fig. 1f), and the spacing labeled in the image is about 0.253 nm, corresponding to (311) plane of Fe₃O₄. Also the inset in Fig. 1f shows the fast Fourier transform pattern of HRTEM image, further proving that the Fe₃O₄ nanosheets are single crystalline.

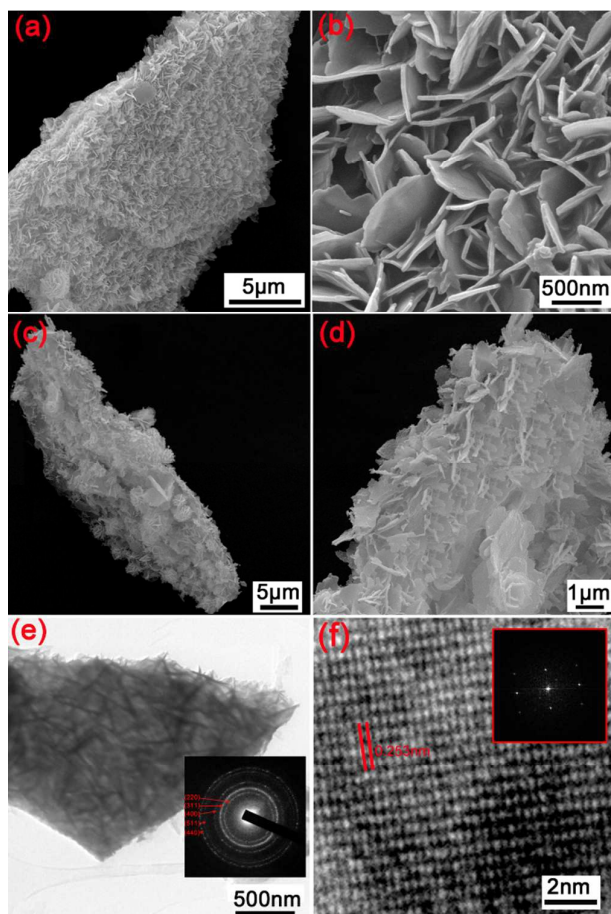


Fig. 1 SEM images of RGO@PDA@iron alkoxide nanosheet arrays (a, b) and graphene@carbon@Fe₃O₄ nanosheet arrays (c, d). TEM image (e), inset showing SAED pattern, and HRTEM image (f), inset showing the fast Fourier transform pattern of graphene@carbon@Fe₃O₄ nanosheet arrays.

The phase structures evolution of the intermediate products obtained at various stages were characterized by X-ray power diffraction (XRD) (Fig. 2a). After GO modified by PDA, the sharp diffraction peak in GO ($2\theta = 10.7$) disappears, and a new broad diffraction peak ($2\theta = 25.3$) appears in the RGO@PDA, indicating the successful introduction of PDA, with accompanied reduction of GO.^[18] After EG-mediated process, a strong diffraction peak appears ($2\theta = 18.7$), which agrees well with the reported iron alkoxide.¹⁹ For graphene@carbon@Fe₃O₄, the detected diffraction peaks can be indexed in the cubic inverse spinel structure of Fe₃O₄ (JCPDS card, file no. 19-0629), indicating the phase transformation from iron alkoxide to Fe₃O₄. Additionally, no characteristic peaks of graphene are observed, suggesting that the Fe₃O₄ could prevent the restacking of the graphene, and the graphene nanosheets are disordered in the graphene@carbon@Fe₃O₄ hybrids. Moreover, the significant structural changes of the carbon framework occurring during each stage were also reflected in their Raman spectra (Fig. 2b). Except two characteristic peaks, corresponding to the D band at ~ 1340 cm⁻¹ and G band at ~ 1590 cm⁻¹, a new peak at 667 cm⁻¹ can be clearly identified. It corresponds to the A_{1g} mode of Fe₃O₄,²⁰

proving the presence of Fe₃O₄ in the hybrids. The intensity ratio of D and G bands (I_D/I_G) in GO (0.76), RGO@PDA (0.84) and graphene@carbon@Fe₃O₄ (0.89) increases gradually, suggesting that GO is reduced to graphene.^{21, 22} The G band shift in carbon-based composite is related to the charge transfer between carbon and other compounds.^{23, 24} Therefore, the observed G band shifts by 5 cm⁻¹ from 1593 cm⁻¹ (RGO@PAD) to 1598 cm⁻¹ (graphene@carbon@Fe₃O₄) can be attributed to the charge transfer from graphene to Fe₃O₄, supporting the formation of Fe-O-C bonds between Fe₃O₄ and graphene sheets.²²

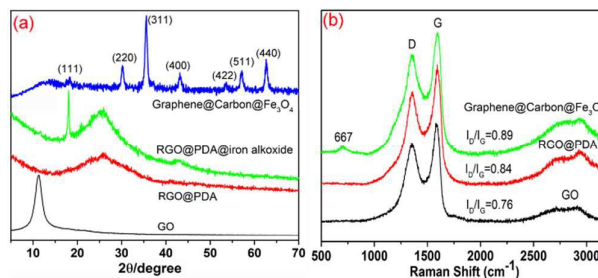


Fig. 2 XRD pattern and Raman spectra of graphene@carbon@Fe₃O₄ nanosheet arrays.

The electromagnetic wave absorption properties were investigated by mixing 30 wt% of the samples with paraffin. The reflection loss (RL) curves of the as-obtained products were calculated by the measured values of the relative complex permittivity and permeability at a given frequency and layer thickness according to the transmission line theory, which is summarized as the following equations:²⁵

$$R_L = 20 \log \left| \frac{Z_{in} - Z_0}{Z_{in} + Z_0} \right| \quad (1)$$

$$Z_{in} = Z_0 \sqrt{\mu_r / \epsilon_r} \tanh \left[j(2\pi f d / c \sqrt{\epsilon_r \mu_r}) \right] \quad (2)$$

where Z_{in} is the input impedance of the absorber, Z_0 is the impedance of free space, and c is the velocity of light in free space, respectively. Fig. 3a showed the calculated RL curves of the as-obtained products in the frequency range of 2~18 GHz with thickness of 2.7 mm. For common applications, it requires the microwave absorbing materials possess a RL value lower than -10 dB which means 90% of incident microwave can be absorbed. Herein, the RL value of GO is very poor and RL was no more than -3 dB, and the RL value of RGO@PDA is still low, although it can reach -11.4 dB. Additionally, the as-prepared flower-like Fe₃O₄ shows the maximum RL of -13.9 dB. Satisfying, the as-prepared 3D graphene@carbon@Fe₃O₄ nanosheet arrays exhibit outstanding microwave absorption properties. The maximum RL can be achieved to -52.8 dB at 9.5 GHz and a broad absorption bandwidth of 3.3 GHz (RL values exceeding -10 dB) covers the 8.1-11.4 GHz. Moreover, the RL of the graphene@carbon@Fe₃O₄ with different thicknesses were also calculated (Fig. 3b). The absorption bandwidth with the RL exceeding -10 dB can be adjusted from 3.8 to 18 GHz for the absorber with thickness of 2.0-5.0 mm. Notably, with increasing thickness, the frequency corresponding to the maximum RL peaks can move toward low frequencies and two RL peaks can be observed with increasing the sample thickness of more than 4.0 mm. This can be well explained by the quarter-wavelength cancellation model.^{26, 27}

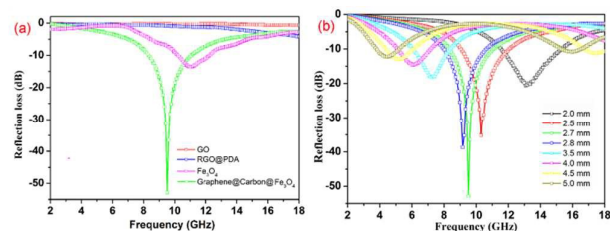


Fig. 3. Comparison of RL between the graphene@carbon@Fe₃O₄ nanosheet arrays, Fe₃O₄, RGO@PDA and GO with a thickness of 2.7 mm (a), and frequency dependence of RL for the graphene@carbon@Fe₃O₄ nanosheet arrays with different thicknesses (b).

To understand the EM absorption enhancement mechanism of the graphene@carbon@Fe₃O₄ nanosheet arrays, the dependence of the complex permittivity and permeability on frequency was investigated. Where the real parts of the complex permittivity (ϵ') and permeability (μ') represent the storage capability of electric and magnetic energy, and imaginary parts the complex permittivity (ϵ'') and permeability (μ'') associate with the loss capability of electric and magnetic energy.²⁸ The complex permittivity and permeability behaviors of graphene@carbon@Fe₃O₄ were studied as shown in Fig. 3. It is noting that the ϵ' and ϵ'' values of graphene@carbon@Fe₃O₄ are larger than those of GO and RGO@PDA (Fig. S3, ESI[†]), indicating the high storage and loss ability of the microwave energy. Furthermore, ϵ' is an expression of polarization ability of a material which mainly arises from dipolar polarization and interfacial polarization at microwave frequency.^{29, 30}

In this case, the increasing ϵ' may be ascribed to the dipolar polarization provided mainly by abundant surface functions and the defects in the graphene@carbon, and the interfacial polarization mainly from the interfaces in Fe₃O₄-carbon-graphene and a large amount of interfaces among Fe₃O₄ nanosheets. These contribute to the dielectric loss according to Debye Theory.³¹ Another contribution to the dielectric loss is from conductivity loss originating from the 3D graphene@carbon@Fe₃O₄, which benefits from the excellent conductivity of graphene@carbon. Fig. 4b showed the frequency dependence of the μ' and μ'' of complex permeability of graphene@carbon@Fe₃O₄. Generally, the imaginary part μ'' is related to the magnetic loss. Thus higher μ'' of graphene@carbon@Fe₃O₄ lead to greater magnetic loss compared with those of GO and RGO@PDA (Fig. S3b, ESI[†]). The enhanced magnetic loss of materials originates mainly from natural resonance, exchange resonance and eddy current loss.³² The values of $\mu''(\mu')^{-2}f^1$ are almost constant in 10-18 GHz (Fig. S4, ESI[†]). Therefore the magnetic loss of graphene@carbon@Fe₃O₄ is mainly originated from natural resonance, exchange resonance in 2-10 GHz and eddy current loss in 10-18 GHz. Moreover, the dielectric loss tangent ($\tan\delta\epsilon = \epsilon''/\epsilon'$) and the magnetic loss tangent ($\tan\delta\mu = \mu''/\mu'$) are two important factors to evaluate microwave absorption properties for an absorber. The largest value of loss tangent indicated the higher capacity of converting electromagnetic waves to other forms of energy.³³ As shown in Fig. 4, the values of $\tan\delta\epsilon$ and $\tan\delta\mu$ for graphene@carbon@Fe₃O₄ are obviously improved compared to these of GO and RGO@PDA shown in Fig. S3,

indicating the high capacity of converting electromagnetic waves to other forms of energy.

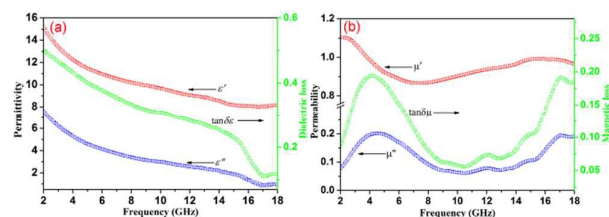


Fig. 4 Frequency dependences of complex permittivity and dielectric loss (a), and complex permeability and magnetic loss (b) for the graphene@carbon@Fe₃O₄ nanosheet arrays.

Based on the above analysis, the dipolar polarization and interfacial polarization will result in strong dielectric losses and take place at high frequency, and eddy current losses which lead to high magnetic losses also take place at high frequency, while natural resonance, exchange resonance work at low frequency. This complementary effect is helpful for the electromagnetic absorption properties, due to the better impedance matching, which is the important key factor for the enhanced microwave absorption properties. The impedance matching degree can be validated by a delta-function method by means of an equation: $\Delta = |\sinh^2(Kfd) - M|$, where K and M can be determined by the relative complex permittivity and complex permeability.³⁴ The smaller delta value implies better EM impedance matching. The delta values, smaller than 0.2, correspond to the RL below -8 dB. Based on the method proposed in ref. 34, the calculated delta value maps of graphene@carbon@Fe₃O₄ is shown in Fig. 5. The large dark blue area indicates the excellent microwave absorption properties.

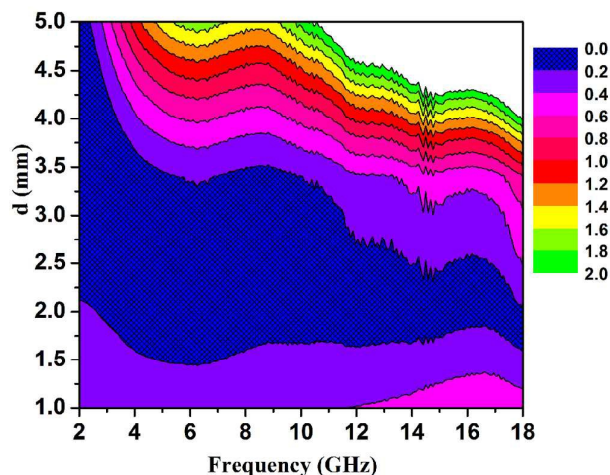


Fig. 5 Calculated delta value map of graphene@carbon@Fe₃O₄ nanosheet arrays.

In addition, EM wave attenuation in the interior of the absorber is another one of the important key factors for a remarkable absorption material. The attenuation constant α , determining the dissipation properties of materials, can be expressed by³⁴

$$\alpha = \frac{\sqrt{2\pi}f}{c} \times \sqrt{(\mu''\epsilon' - \mu'\epsilon'') + \sqrt{(\mu''\epsilon' - \mu'\epsilon'')^2 + (\epsilon'\mu'' + \epsilon''\mu')^2}} \quad (3)$$

where f and c are the frequency and velocity of light, respectively. The frequency dependence of α for GO, RGO@PDA and graphene@carbon@Fe₃O₄ is displayed in Fig. 5. It is clearly seen that the graphene@carbon@Fe₃O₄ have the largest α in the entire frequency range, suggesting its outstanding absorption.

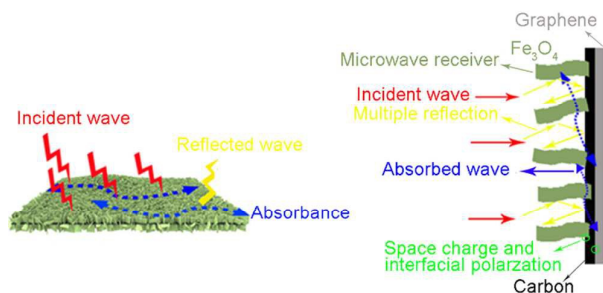


Fig. 6 Schematic illustration of a plausible electromagnetic wave absorption mechanism for the graphene@carbon@Fe₃O₄ nanosheet arrays.

On the basis of the above discussion, a plausible electromagnetic wave absorption mechanism for the 3D graphene@carbon@Fe₃O₄ nanosheet arrays is proposed, as depicted in Fig. 6. When the graphene@carbon@Fe₃O₄ is subjected to electromagnetic wave radiation, the Fe₃O₄ nanosheets grown on the surfaces of graphene@carbon are expected to act as antennae receivers allowing electromagnetic waves to penetrate into the interior of the absorber as much as possible the electromagnetic wave energy transfers in the form of microcurrent.³⁵ The Fe₃O₄ nanosheets can convert more and more electromagnetic energy to microcurrent, due to the increase in impedance matching. The microwave current generated is then required to transmit along one sheet-like structure to another. During transmission, the graphene@carbon serves as an electrically conductive network. A large part of the electric energy could be attenuated due to the resistance of the graphene@carbon. Moreover, the special structure leads to defects and multi-interfaces (carbon-Fe₃O₄, Fe₃O₄-Fe₃O₄ and carbon-graphene), which can cause additional space charge polarization and interfacial polarization with the associated relaxation.³⁶⁻³⁸ These also could stimulate the electron polarization, favoring the attenuation electromagnetic wave.

Conclusions

In summary, we developed an efficient strategy to fabricate a 3D architecture of graphene@carbon@Fe₃O₄ nanosheet arrays by a mussel-inspired polydopamine adhesive, in which Fe₃O₄ nanosheet were almost grown perpendicularly on both surfaces of graphene sheets. After introducing Fe₃O₄ nanosheet arrays with accompanied reduction of GO into graphene, the 3D architectures exhibit outstanding EM absorption properties. The maximum reflection loss value can reach -52.8 dB at 9.5 GHz with the sample thickness of 2.7 mm. The improved EM wave absorption properties is realized by the synergistic effects of magnetic loss in Fe₃O₄ nanosheet

arrays and dielectric loss in graphene@carbon. Furthermore, the synthesis strategy presented here can be expanded as a facile approach to synthesizing related graphene-based 3D nanostructures for functional design and applications.

Notes and references

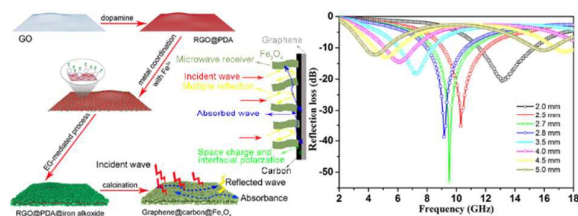
- 1 Y. Zhang, Y. Huang, T. F. Zhang, H. C. Chang, P. S. Xiao, H. H. Chen, Z. Y. Huang and Y. S. Chen, *Adv. Mater.*, 2015, **12**, 2049.
- 2 M. Q. Ning, M. M. Lu, J. B. Li, Z. Chen, Y. K. Dou, C. Z. Wang, F. Rehman, M. S. Cao and H. B. Jin, *Nanoscale*, 2015, 15734.
- 3 B. Wen, M. S. Cao, M. M. Lu, W. Q. Cao, H. L. Shi, J. Liu, X. X. Wang, H. B. Jin, X. Y. Fang, W. Z. Wang and J. Yuan, *Adv. Mater.*, 2014, **26**, 3484.
- 4 J. W. Liu, R. C. Che, H. J. Chen, F. Zhang, F. Xia, Q. S. Wu and M. Wang, *Small*, 2012, **8**, 1214.
- 5 X. H. Li, J. Feng, Y. P. Du, J. T. Bai, H. M. Fan, H. L. Zhang, Y. Peng and F. S. Li, *J. Mater. Chem. A*, 2015, **3**, 5535.
- 6 L. Wang, Y. Huang, C. Li, J. J. Chen and X. Sun, *Phys. Chem. Chem. Phys.*, 2015, **17**, 5818.
- 7 L. Wang, Y. Huang, X. Sun, H. J. Huang, P. B. Liu, M. Zong and Y. Wang, *Nanoscale*, 2014, **6**, 3157.
- 8 H. Zhang, A. J. Xie, C. P. Wang, H. S. Wang, Y. H. Shen and X. Y. Tian, *J. Mater. Chem. A.*, 2013, **1**, 8547.
- 9 Y. L. Ren, H. Y. Wu, M. M. Lu, Y. J. Chen, C. L. Zhu, P. Gao, M. S. Cao, C. Y. Li and Q. Y. Ouyang, *ACS Appl. Mater. Interfaces*, 2012, **4**, 6436.
- 10 H. L. Xu, H. Bi, R. B. Yang and *J. Appl. Phys.*, 2012, **111**, 07A522.
- 11 V. K. Singh, A. Shukla, M. K. Patra, L. Saini, R. K. Jani, S. R. Vadera and N. Kumar, *Carbon*, 2012, **50**, 2202.
- 12 Y. L. Ren, C. L. Zhu, S. Zhang, C. Y. Li, Y. J. Chen, P. Gao, P. P. Yang and Q. Y. Ouyang, *Nanoscale*, 2013, **5**, 12296.
- 13 X. H. Li, H. B. Yi, J. W. Zhang, J. Feng, F. S. Li, D. S. Xue, H. L. Zhang, Y. Peng and N. J. Mellors, *J. Nanopart. Res.*, 2013, **15**, 1472.
- 14 X. N. Chen, F. C. Meng, Z. W. Zhou, X. Tian, L. M. Shan, S. B. Zhu, X. L. Xu, M. Jiang, L. Wang, D. Hui, Y. Wang, J. Lu and J. H. Gou, *Nanoscale*, 2014, **6**, 8140.
- 15 L. Q. Xu, W. J. Yang, K. Neoh, E. Kang and G. D. Fu, *Macromolecules*, 2010, **43**, 8336.
- 16 H. Lee, S. M. Dellatore, W. M. Miller and P. B. Messersmith, *Science*, 2007, **318**, 426.
- 17 J. Ryu, S. H. Ku, H. Lee and C. B. Park, *Adv. Funct. Mater.*, 2010, **20**, 2132.
- 18 L. Q. Xu, W. J. Yang, K. G. Neoh, E. T. Kang and G. D. Fu, *Macromolecules*, 2010, **43**, 8336.
- 19 L. S. Zhong, J. S. Hu, H. P. Liang, A. M. Cao, W. G. Song and L. J. Wan, *Adv. Mater.*, 2006, **18**, 2426.
- 20 G. Zhou, D. W. Wang, F. Li, L. Zhang, N. Li, Z. S. Wu, L. Wen, G. Q. Lu and H. M. Cheng, *Chem. Mater.*, 2010, **22**, 5306.
- 21 K. Singh, A. Ohlan, V. H. Pham, R. Balasubramanian, S. Varshney, J. Jang, S. H. Hur, W. M. Choi, M. Kumar, S. K. Dhawan, B. S. Kong and J. S. Chung, *Nanoscale*, 2013, **5**, 2411.
- 22 X. Xu, H. Li, Q. Q. Zhang, H. Hu, Z. B. Zhao, J. H. Li, J. Y. Li, Y. Qiao and Y. Gogotsy, *ACS Nano*, 2015, **9**, 3969.
- 23 J. Zhou, H. Song, L. Ma and X. Chen, *RSC Adv.*, 2011, **1**, 782.
- 24 N. Zubir, C. Yacou, J. Motuzas, X. Zhang and J. Costa, *Sci. Rep.*, 2014, **4**, 4594.
- 25 E. Michielssen, J. M. Sajer, S. Ranjithan and R. Mittra, *IEEE Trans. Microwave Theory Tech.*, 1993, **41**, 1024.
- 26 C. Wang, X. Han, X. Zhang, S. Hu, T. Zhang, J. Wang, Y. Du, X. Wang and P. Xu, *J. Phys. Chem. C*, 2010, **114**, 14826-14830.
- 27 B. Zhao, G. Shao, B. Fan, W. Zhao and R. Zhang, *Phys. Chem. Chem. Phys.*, 2015, **17**, 2531.

ARTICLE

Journal Name

- 28 Y. C. Du, W. W. Liu, R. Qiang, Y. Wang, X. J. Han, J. Ma and P. Xu, *ACS Appl. Mater. Inter.*, 2014, **6**, 12997.
- 29 Q. L. Liu, D. Zhang and T. X. Fan, *Appl. Phys. Lett.*, 2008, **93**, 013110.
- 30 P. C. P. Watts, W. K. Hsu, A. Barnes and B. Chambers, *Adv.Mater.*, 2003, **15**, 600.
- 31 B. Wen, M. S. Cao, Z. L. Hou, W. L. Song, L. Zhang, M. M. Lu, H. B. Jin, X. Y. Fang, W. Z. Wang and J. Yuan, *Carbon*, 2013, **65**, 124.
- 32 F. S. Wen, F. Zhang and Z. Y. Liu, *J. Phys. Chem. C*, 2011, **115**, 14025.
- 33 X. M. Zhang, G. B. Ji, W. Liu, B. Quan, X. H. Liang, C. M. Shang, Y. Cheng and Y. W. Du, *Nanoscale*, 2015, **7**, 12932.
- 34 Z. Ma, C. T. Cao, Q. F. Liu and J. B. Wang, *Chin. Phys. Lett.*, 2012, **29**, 038401.
- 35 R. F. Zhuo, L. Qiao, H. T. Feng, J. T. Chen and D. Yan, *J. Appl. Phys.*, 2008, **104**, 094101.
- 36 M. Zong, Y. Huang, Y. Zhao, X. Sun, C. H. Qu, D. D. Luo and J. B. Zheng, *RSC Adv.*, 2013, **3**, 23638.
- 37 M. Zong, Y. Huang, H. W. Wu, Y. Zhao, Q. F. Wang and X. Sun, *Mater. Lett.*, 2014, **114**, 52.
- 38 M. Zong, Y. Huang, N. Zhang and H. W. Wu, *J. Alloy. Compd.*, 2015, **644**, 491.

A table of contents entry



Fe_3O_4 nanosheet arrays can grow on graphene by a mussel-inspired polydopamine adhesive towards remarkable enhancement in electromagnetic absorptions.